25. K. B. Min, J. Rutqvist, C. F. Tsang, L. Jing, *Int. J. Rock Mech. Min. Sci.* **41**, 1191–1210 (2004).
26. D. Richter, S. A. Billings, *New Phytol.* **206**, 900–912 (2015).
27. E. T. Cleaves, A. E. Godfrey, O. P. Bricker, *Geol. Soc. Am. Bull.* **81**, 3015–3032 (1970).
28. N. Barton, *Rock Quality, Seismic Velocity, Attenuation and Anisotropy* (Taylor and Francis Group, London, 2006).
29. W. S. Holbrook *et al*., *Earth Surf. Process. Landf.* **39**, 366–380 (2014).
30. A. Nur, G. Simmons, *Earth Planet. Sci. Lett.* **7**, 183–193 (1969).
31. O. O. Blake, D. R. Faulkner, A. Rietbrock, *Pure Appl. Geophys.* **170**, 493–505 (2013).
32. G. E. Archie, *Trans. Am. Inst. Min. Metall. Pet. Eng.* **146**, 54–62 (1942).
33. D. W. Schwartzman, T. Volk, *Nature* **340**, 457–460 (1989).

ACKNOWLEDGMENTS

This study was supported by the NSF Experimental Program to Stimulate Competitive Research (award EPS-1208909), the U.S. Army Research Office (grant W911NF-14-1-0037), NSF Earth Sciences (awards EAR-0724960 to the University of Colorado–Boulder and EAR-1331846 to Duke University), and the NSF Critical Zone Observatory Network. Poly3D software was provided by Schlumberger. 3DMove software was provided by Midland Valley Software. Geophysical data presented in this paper are available through the Wyoming Center for Environmental Hydrology and Geophysics data repository at http://ecoinfo.wygisc.org/data-archive#PB_CCZO_BCCZO. The authors thank the editor and three anonymous reviewers for their suggestions.

SUPPLEMENTARY MATERIALS

www.sciencemag.org/content/350/6260/534/suppl/DC1
Materials and Methods
Figs. S1 to S10
Tables S1 to S3
References (*34*–*55*)

27 March 2015; accepted 25 August 2015
10.1126/science.aab2210

MAGNETISM

Mobile metallic domain walls in an all-in-all-out magnetic insulator

Eric Yue Ma,[1,2]* Yong-Tao Cui,[1]* Kentaro Ueda,[3,4]* Shujie Tang,[1,5] Kai Chen,[6] Nobumichi Tamura,[7] Phillip M. Wu,[1] Jun Fujioka,[3,4] Yoshinori Tokura,[3,4]† Zhi-Xun Shen[1,2]†

Magnetic domain walls are boundaries between regions with different configurations of the same magnetic order. In a magnetic insulator, where the magnetic order is tied to its bulk insulating property, it has been postulated that electrical properties are drastically different along the domain walls, where the order is inevitably disturbed. Here we report the discovery of highly conductive magnetic domain walls in a magnetic insulator, $Nd_2Ir_2O_7$, that has an unusual all-in-all-out magnetic order, via transport and spatially resolved microwave impedance microscopy. The domain walls have a virtually temperature-independent sheet resistance of ~1 kilohm per square, show smooth morphology with no preferred orientation, are free from pinning by disorders, and have strong thermal and magnetic field responses that agree with expectations for all-in-all-out magnetic order.

Magnetic order, in particular antiferromagnetism, often accompanies metal-insulator transitions (MITs), during which metallic materials abruptly become insulating or semiconducting at certain critical temperatures (*1*). Whether metallic behavior can be recovered in these magnetic insulators at magnetic domain walls (DWs), where the order is inevitably disturbed, is a long-standing question that is widely addressed theoretically but remains elusive experimentally (*2*–*5*). A related but distinct situation is that of conductive ferroelectric DWs in ferroelectric insulators, the discovery of which has opened a broad field of research dedicated to understanding the fundamental mechanism, as well as making practical DW-based devices (*6*–*9*). However, among the vast array of magnetic insulators, no conductive magnetic DW has been firmly identified so far. Recently, bulk measurements have provided signatures of DW conduction in the low-temperature insulating phase of $Nd_2Ir_2O_7$ (*10*), a candidate for the exotic "Weyl semimetal" with an unusual all-in-all-out magnetic order (*11*–*16*). Here we combine bulk measurements with local-conductivity–measuring microwave impedance microscopy (MIM) to directly resolve highly conductive DWs in $Nd_2Ir_2O_7$ in real space. These results rule out alternative contributions and thus provide evidence for a realization of conduction due to the discontinuity of magnetic order.

$Nd_2Ir_2O_7$ is a pyrochlore iridate in which the electronic states near Fermi energy are dominated by t_{2g} electrons from Ir atoms (*17*). It undergoes a MIT at a Néel temperature T_N ~32 K (Fig. 1A), with a concomitant all-in-all-out (AIAO) magnetic order developing for the Ir magnetic moments (*14*, *18*, *19*): The Ir moments at the four vertices of each corner-sharing tetrahedron all point either inward or outward in an alternating manner (Fig. 1B). This unusual magnetic order is a ferroic order of magnetic octupole and preserves the symmetry of the underlying lattice (*13*). For a given lattice, there are two and only two distinct variations of the order: all-in-all-out (AIAO) and all-out-all-in (AOAI). They represent opposite magnetic octupoles and are interchanged with each other by time-reversal transformation; by contrast, their electronic properties should be identical in the absence of external perturbations.

Nonetheless, abnormal conduction can happen at the boundaries between AIAO and AOAI domains (i.e., magnetic DWs), as hinted by macroscopic transport measurements (*10*): The resistance of the same polycrystalline sample at 4.5 K after cooling from above T_N in zero field (ZFC or "untrained") can be more than a factor of 200 smaller than that cooled in a 9-T field (FC or "trained") (Fig. 1A). One may attribute the extra conduction to DWs, with field cooling resulting in fewer magnetic domains, fewer DWs, and thus higher overall resistance. However, alternative explanations, including history dependence of the bulk and grain boundaries, cannot be ruled out by these macroscopic measurements.

We confirm the existence of highly conductive magnetic DWs by direct imaging with MIM, a scanning probe technique that senses local conductivity by measuring tip-sample impedance at ~1 GHz (*20*–*22*): More conductive regions screen the microwave electric field better, resulting in a smaller tip-sample impedance. Working at high frequency eliminates the need of a back electrode and a complete current path, making MIM ideal for bulk insulating samples (*23*). Figure 1C is an 18 μm by 18 μm MIM scan of a polished $Nd_2Ir_2O_7$ polycrystal surface (fig. S1A) at 4.7 K after cooling in zero field (untrained). Smooth curvilinear features that are much more conductive than the bulk exist in all grains, with an apparent width of ~100 nm, similar to the spatial resolution of MIM in this particular experiment (fig. S2). They are continuous within individual grains, show no preferred orientations, and either form closed loops or terminate at the grain boundaries, but they never form vertices. As a result, each grain is divided into regions that can be assigned using only two labels, as expected for AIAO order, which has only two variations. Interestingly, many DWs from adjacent grains are in close proximity at the grain boundaries (yellow arrows in Fig. 1C). Such proximity may facilitate transport across grain boundaries and enhance the DW contribution to the measured conductance in macroscopic polycrystalline samples (*10*). We stress here that the

[1]Geballe Laboratory for Advanced Materials (GLAM), Stanford University, Stanford, CA, USA. [2]Department of Applied Physics, Stanford University, Stanford, CA, USA. [3]Department of Applied Physics, University of Tokyo, Tokyo, Japan. [4]RIKEN Center for Emergent Matter Science (CEMS), Saitama, Japan. [5]State Key Laboratory of Functional Materials for Informatics, Shanghai Institute of Microsystem and Information Technology (SIMIT), Shanghai, China. [6]Center for Advancing Materials Performance from the Nanoscale (CAMP-Nano), State Key Laboratory for Mechanical Behavior of Materials, Xi'an Jiaotong University, Xi'an, China. [7]Advanced Light Source (ALS), Lawrence Berkeley National Laboratory, Berkeley, CA, USA.
*These authors contributed equally to this work. **†Corresponding author. E-mail: tokura@riken.jp (Y.T.); zxshen@stanford.edu (Z.-X.S.)**

grain boundaries themselves are as insulating as the bulk; thus, their contribution to the extra conduction can be ruled out (fig. S1, B and C). Notably, while the domains are stable against heating to below T_N, they are completely randomized after a thermal cycle to above T_N (Fig. 1D) (*24*), indicating that they are tied to the AIAO order and are not pinned by quenched disorders. It also implies that the system randomly evolves into

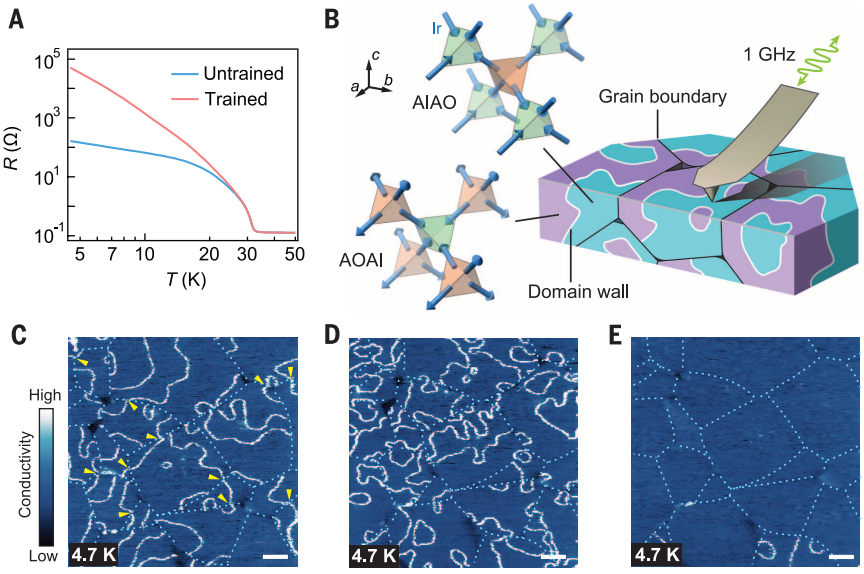

Fig. 1. Microwave impedance microscopy (MIM) reveals conductive magnetic domain walls in $Nd_2Ir_2O_7$. (**A**) Four-terminal resistance of a macroscopic polycrystal taken during zero-field warming after cooling in zero field (untrained) and 9 T field (trained) from 50 K. (**B**) Illustration of MIM scanning setup on polished polycrystal $Nd_2Ir_2O_7$, showing the spin configuration of AIAO order and its AIAO/AOAI variations. Domain walls can exist between the two variations. (**C**) An 18 μm by 18 μm MIM image of a polished $Nd_2Ir_2O_7$ polycrystal surface, after zero-field cooling from 40 to 4.7 K. A higher MIM signal corresponds to a higher local conductivity. The dotted lines are grain boundaries and the dark spots are voids between grains, which can be identified in higher-temperature scans (fig. S1, B and C). Curvilinear features much more conductive than the bulk are observed in all grains and are identified as AIAO magnetic domain walls. They either form closed loops or terminate at the grain boundaries, sometimes in close proximity (yellow arrows). (**D**) Same region (with a small offset) after a thermal cycle to 40 K and back to 4.7 K in zero field, showing randomized domains. (**E**) Same region after a thermal cycle to 40 K and cooling back to 4.7 K in 9 T. Most grains become single-domain, agreeing with transport. Scale bars: 2 μm.

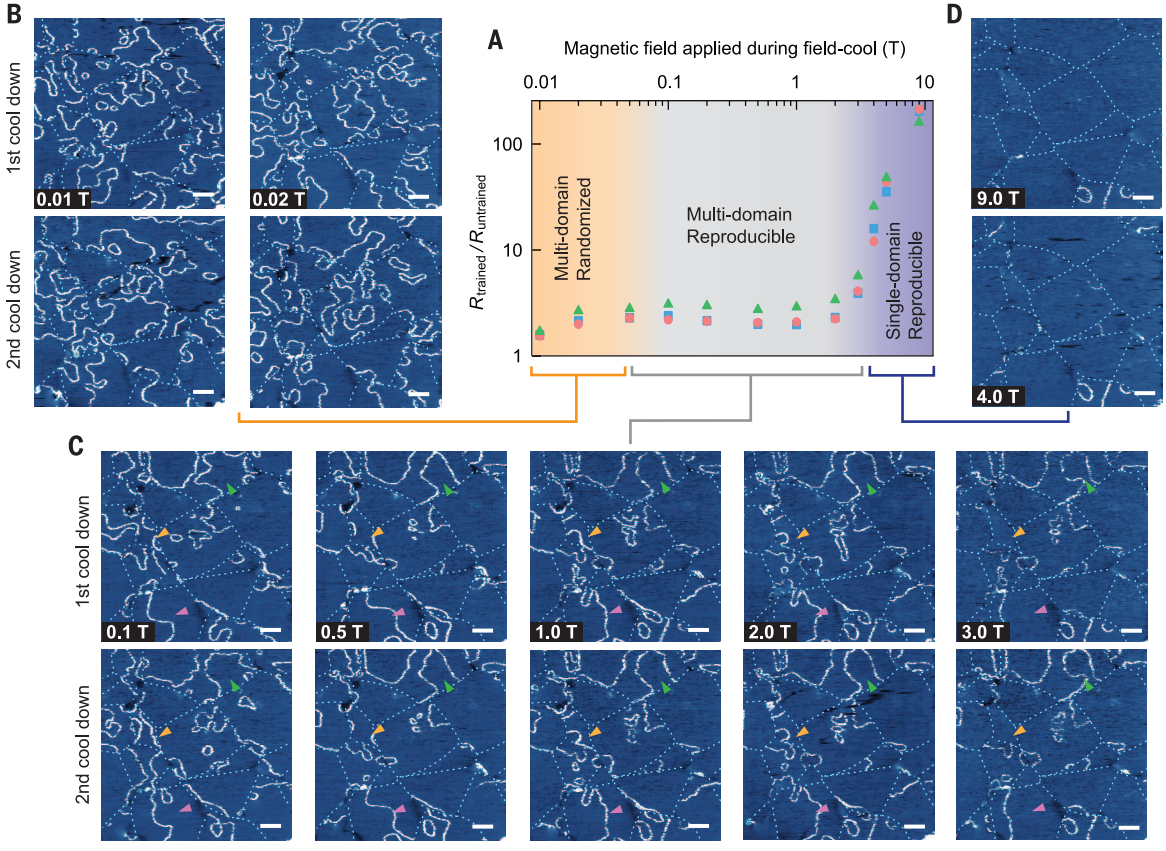

Fig. 2. MIM images for various values of magnetic field applied during cool-down. A multidomain ground state reproducible between thermal cycles is recovered if cooled in 0.1 T or higher. (**A**) Ratio of final resistance at 4.5 K after cooling in various fields versus cooling in zero field. Data from three samples are shown. (**B**) MIM images of the same region as in Fig. 1 after two consecutive thermal cycles from 40 to 4.7 K in 0.01 and 0.02 T, showing abundant DWs and randomized domain configurations between thermal cycles. (**C**) Same region after cooling in 0.1 to 3.0 T, showing reduced number of DWs and the recovery of a reproducible multidomain ground state. Colored arrows highlight dependence of DW configuration on field magnitude. (**D**) Same region after cooling in 4.0 and 9.0 T, showing rapid disappearance of DWs in most but not all grains. Scale bars: 2 μm.

one of the many near-degenerate multidomain states, with substantial energy barriers in between. Finally, most conductive features disappear after cooling in a 9-T field (trained), in agreement with transport results. The evidence above supports the conductive curves being AIAO magnetic DWs, with conductivity much enhanced in comparison to the bulk.

A multidomain ground state reproducible between thermal cycles is recovered if cooled in a field of ≥0.1 T, with an unexpected dependence on the field magnitude (Fig. 2). For cooling in very small fields (≲0.02 T), the DWs remain abundant and randomized between thermal cycles as in the ZFC case (Fig. 2B). As the field is increased to ~0.1 T, the number of DWs within each grain decreases; in the meantime, DW configuration becomes mostly reproducible between thermal cycles, indicating a well-defined multidomain ground state (Fig. 2C). Whereas the number of DWs remains largely stable up to 3 T (corresponding to the plateau of FC/ZFC resistance ratio in Fig. 2A), the detailed DW configuration changes unmistakably as a function of field magnitude (compare, for example, regions marked by colored arrows in Fig. 2C). This indicates competition of AIAO and AOAI coupled to local degrees of freedom—for example, strain via the predicted magnetostriction effect (*13*). Above ~3 T, a single-domain ground state quickly becomes favorable (Fig. 2D), likely due to the field response of the much larger Nd moments, coupled to Ir moments through f-d coupling (*12*, *14*, *15*, *25*), and the resistance increases rapidly (Fig. 2A). Nevertheless, a few grains remain multidomain even if cooled in 9 T, the origin of which can be well explained with crystal orientation dependence, as discussed below.

The field response of the DWs at a fixed temperature demonstrates the expected crystal orientation dependence of AIAO magnetic order. Figure 3A shows the evolution of DWs as an out-of-plane magnetic field is increased from 0 to 9 T, at 4.7 K after ZFC. Figure 3C shows the out-of-plane crystal orientation of the same area obtained with x-ray microdiffraction (μXRD) (*26*). DWs disappear abruptly at grain-specific critical fields that depend on the crystal orientation. The first grain to become single-domain at 3 T (blue triangle in Fig. 3A) has an out-of-plane direction closest to [111] (dark blue color in Fig. 3C). Most other grains subsequently transition between 4

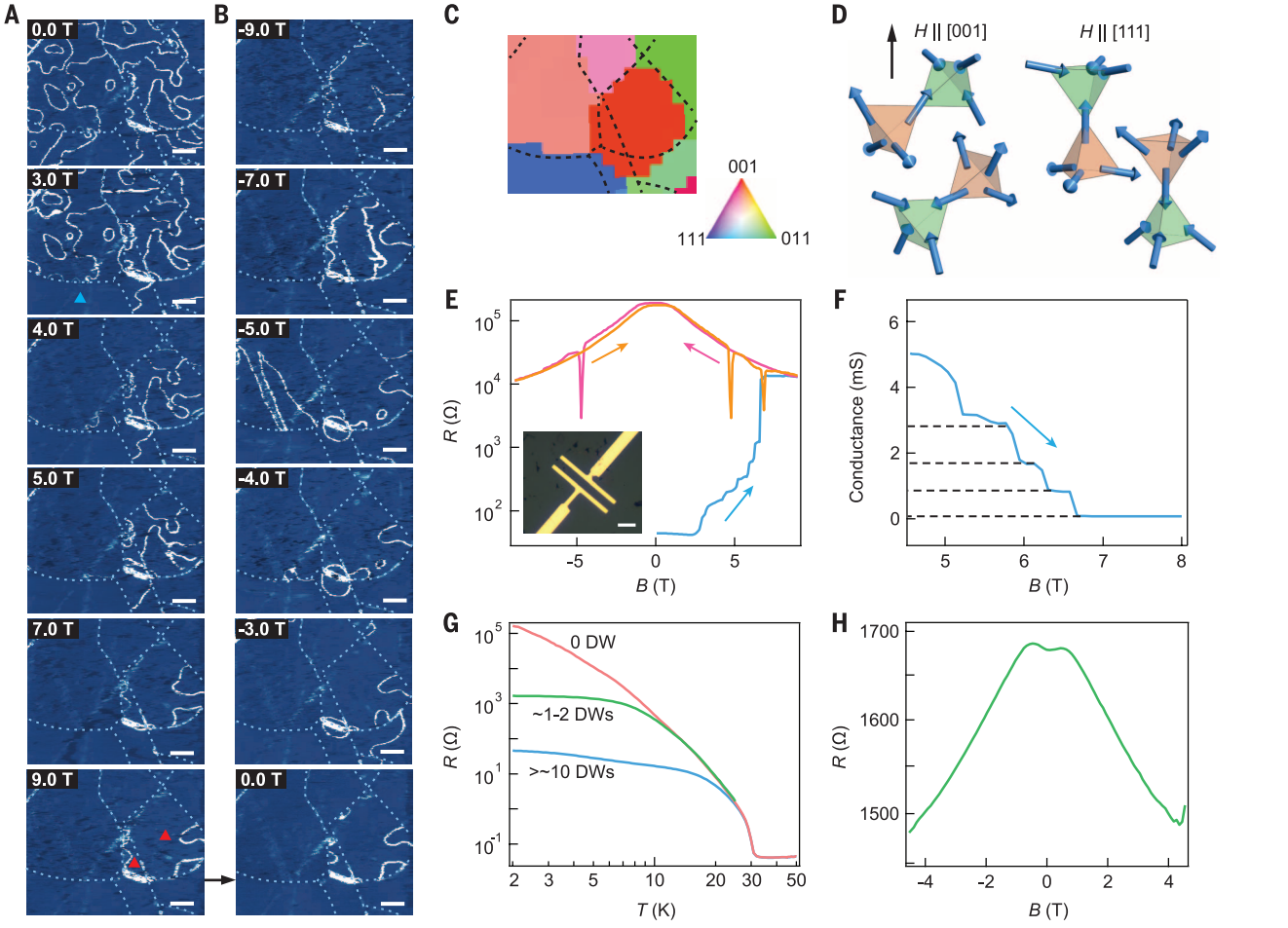

Fig. 3. Field-dependent domain evolution at low temperature and DW sheet resistance measured with microelectrodes. (**A**) Field dependence of DWs at 4.7 K. The first grain to become single-domain is marked by a blue triangle, and the two grains that remain multidomain at 9 T by red triangles. (**B**) The same region during subsequent field sweeps back to 0 T and then to −9 T, showing transient DW formation during domain reversal. (**C**) Out-of-plane crystal orientation of the same area obtained with μXRD, as indicated by the tricolor map. The blue and red grains in (A) have an out-of-plane orientation closest to [111] and [001], respectively. (**D**) Illustration of field-induced spin canting with a field along the [111] and [001] direction for AIAO and AOAI configurations: The largest difference is generated for the [111] case, while the effects are equivalent for the [001] case, consistent with data in (A) and (C). (**E**) Typical resistance versus magnetic field of a microelectrode device (inset) at 2 K when sweeping the field from 0 to 9 T (blue), 9 to −9 T (magenta), and −9 to 9 T (orange) after a ZFC. Discrete resistance jumps and sharp resistance minimums are shown. Scale bar (inset): 5 μm. (**F**) The initial sweep (blue) in (E) converted to conductance, showing staircase-like conductance drops. Sheet resistance of DWs averaged over mesoscopic lengths is thus estimated to be ~1 kilohm/sq. (**G**) Temperature dependence of resistance for various initial states taken during zero-field warming, showing the virtually temperature-independent conduction property of a few DWs. (**H**) Magnetoresistance of a few DWs at 2 K. The contribution from bulk magnetoresistance is negligible and is subtracted as a parallel resistor. Scale bars (A and B): 2 μm.

and 7 T. The two grains that remain multidomain even at 9 T (red triangles in Fig. 3A) are closest to [001] (red color in Fig. 3C). This is in excellent agreement with expectations from the symmetry of AIAO order: The magnetic field along [111] gives rise to the largest difference in spin canting between AIAO and AOAI, whereas the field along [001] gives rise to equivalent perturbations in the two variations, connected by a simple 90° rotation along [001] (Fig. 3D) (*13*). Therefore, the critical field should be smallest when applied in the [111] direction and largest in the [001] direction, regardless of the detailed mechanism. The grain that remains multidomain in Figs. 1 and 2 is also close to [001], as confirmed by μXRD data (fig. S3). These observations further corroborate the identification of the conductive curves as AIAO DWs.

The sheet resistance of a single DW averaged over mesoscopic lengths is ~1 kilohm/sq. This value was obtained by fabricating microelectrodes on the sample surface to measure transport directly across a few grains [Fig. 3E (inset) and fig. S4A]. Figure 3E shows a typical resistance-versus-magnetic-field plot of such devices at 2 K following a ZFC. During the initial field sweep from 0 to 9 T (blue trace), resistance increases in discrete steps, reflecting the abrupt disappearance of DWs in each grain contacted by electrodes (Fig. 3A). By converting resistance into conductance, we notice that the decreases in conductance associated with each jump are markedly similar, at ~1 mS (Fig. 3F and fig. S4B). Assuming one or two DWs in each grain and an average effective aspect ratio on the order of 1 (fig. S4A), we conclude that the sheet resistance of the AIAO DW averaged over mesoscopic lengths is ~1 kilohm/sq. This value is consistent with the three-dimensional–averaged DW conductivity obtained by terahertz spectroscopy measurements (*10*), assuming an average DW spacing of 2 μm.

The sheet resistance of DWs has very weak temperature dependence at low temperatures and shows substantial negative magnetoresistance. We first develop a method to reliably prepare a few DWs across the electrodes by capturing transient DW formation. Following the staircase-like trace during the initial field sweep, sharp resistance minimums occur for subsequent sweeps (magenta and orange trace in Fig. 3E), because of transient DW formation during the rapid grain-wise domain reversals (from AIAO to AOAI, or vice versa), as also seen in MIM images (Fig. 3B). These sharp reversals ensure that if the field sweep is stopped immediately when a resistance minimum occurs, only one or two DWs will typically exist across the electrodes. We find that these artificially created DWs are stable against temperature and magnetic field sweeps, as long as we stay below T_N and the critical field. The few DWs obtained this way show ohmic behavior (fig. S5) and a virtually temperature-independent sheet resistance until overwhelmed by bulk conduction at high temperatures (Fig. 3G). Indeed, the resistance of multiple DWs increases by only ~10% when cooling from 0.6 K to 35 mK (fig. S6), indicating a gapless electronic structure that is moderately localized owing to, for example, the slowly varying DW orientation. The gapless nature of the DWs is further corroborated by thermal power measurements (fig. S7). The DW resistance shows substantial negative magnetoresistance for fields up to ±4 T (Fig. 3H). A small minimum near zero-field resembles weak antilocalization, as commonly seen in materials with strong spin-orbit coupling (*27*).

The metallic DWs result from mid-gap states that are extended within the DW plane but are localized perpendicular to it. Such "defect states" are generally present, theoretically, if the magnetically disordered state is metallic and the disturbance to the order parameter is sharp (*2*–*6*, *28*). Indeed, metallic DWs are not observed in other $Ln_2Ir_2O_7$ (where Ln is Sm, Eu, etc.) with similar magnetic order: Unlike $Nd_2Ir_2O_7$, they are all semiconducting instead of metallic above the magnetic transition temperature (*12*). The highly anisotropic AIAO order is also expected to give rise to sharp DWs in $Nd_2Ir_2O_7$: The spins are locked firmly to [111] and equivalent crystal orientations via spin-orbit coupling and cannot rotate continuously across magnetic domains (*15*). The resulting sharp DWs represent an abrupt disturbance of magnetic order parameter and can host mid-gap states well separated from bulk states. The picture of magnetic-superlattice–driven MIT (Slater insulator) is not applicable here because AIAO order preserves the symmetry of the underlying pyrochlore lattice (*29*).

In the particular case of iridates, the above generic picture may be captured by the interface states near an exotic "Weyl semimetal" phase. The AIAO order is predicted to host a "Weyl semimetal" phase near the MIT with "Weyl fermions" in the bulk and "Fermi arc" states at the surfaces (*11*), as well as interfaces between AIAO and AOAI domains (*30*). At temperatures much lower than the transition, the bulk becomes insulating as the "Weyl fermions" annihilate and the "Fermi arc" states disappear at the surfaces. Nonetheless, mid-gap states are shown to survive at the magnetic DWs (*30*). Our observation—namely, of metallic DWs and insulating surfaces and grain boundaries—is consistent with the prediction of this theory. A conclusive confirmation, however, requires more systematic studies.

The highly conductive, mobile DWs show no preferred orientation, are free from pinning by disorders, and can be easily manipulated via heat, magnetic field, and probably strain and geometry. They provide an excellent platform, scientifically, for studying exotic emergent phenomena at interfaces, and practically, for DW-based memory devices that can be read electronically without relying on magnetic junctions (*31*). Similar properties may be present in other materials with a true MIT and a highly anisotropic magnetic order, commonly seen in heavy-element materials with large spin-orbit coupling.

REFERENCES AND NOTES

1. M. Imada, A. Fujimori, Y. Tokura, *Rev. Mod. Phys.* **70**, 1039–1263 (1998).
2. D. Poilblanc, T. M. Rice, *Phys. Rev. B* **39**, 9749–9752 (1989).
3. H. J. Schulz, *Phys. Rev. Lett.* **64**, 1445–1448 (1990).
4. M. Inui, P. B. Littlewood, *Phys. Rev. B* **44**, 4415–4422 (1991).
5. C. Nayak, F. Wilczek, *Phys. Rev. Lett.* **78**, 2465–2468 (1997).
6. J. Seidel *et al*., *Nat. Mater.* **8**, 229–234 (2009).
7. D. Meier *et al*., *Nat. Mater.* **11**, 284–288 (2012).
8. W. Wu, Y. Horibe, N. Lee, S.-W. Cheong, J. R. Guest, *Phys. Rev. Lett.* **108**, 077203 (2012).
9. G. Catalan, J. Seidel, R. Ramesh, J. F. Scott, *Rev. Mod. Phys.* **84**, 119–156 (2012).
10. K. Ueda *et al*., *Phys. Rev. B* **89**, 075127 (2014).
11. X. Wan, A. M. Turner, A. Vishwanath, S. Y. Savrasov, *Phys. Rev. B* **83**, 205101 (2011).
12. K. Matsuhira, M. Wakeshima, Y. Hinatsu, S. Takagi, *J. Phys. Soc. Jpn.* **80**, 401442857 (2011).
13. T.-H. Arima, *J. Phys. Soc. Jpn.* **82**, 40144963 (2013).
14. K. Ueda *et al*., *Phys. Rev. Lett.* **109**, 136402 (2012).
15. K. Tomiyasu *et al*., *J. Phys. Soc. Jpn.* **81**, 40144618 (2012).
16. K. Matsuhira, M. Tokunaga, M. Wakeshima, Y. Hinatsu, S. Takagi, *J. Phys. Soc. Jpn.* **82**, 023706 (2013).
17. D. Pesin, L. Balents, *Nat. Phys.* **6**, 376–381 (2010).
18. K. Matsuhira *et al*., *J. Phys. Soc. Jpn.* **76**, 043706 (2007).
19. H. Sagayama *et al*., *Phys. Rev. B* **87**, 100403 (2013).
20. W. Kundhikanjana, K. Lai, M. A. Kelly, Z. X. Shen, *Rev. Sci. Instrum.* **82**, 033705 (2011).
21. Y. Yang *et al*., *J. Micromech. Microeng.* **22**, 115040 (2012).
22. E. Y. Ma *et al*., *Nat. Commun.* **6**, 7595 (2015).
23. K. Lai, W. Kundhikanjana, M. A. Kelly, Z. X. Shen, *Appl. Phys. Lett.* **93**, 123105 (2008).
24. The characteristics of the domain patterns remain stable for a cooling rate between 0.5 and 25 K/min.
25. K. Ueda *et al*., *Phys. Rev. Lett.* **115**, 056402 (2015).
26. M. Kunz *et al*., *Rev. Sci. Instrum.* **80**, 035108 (2009).
27. T. Koga, J. Nitta, T. Akazaki, H. Takayanagi, *Phys. Rev. Lett.* **89**, 046801 (2002).
28. J. Salafranca, R. Yu, E. Dagotto, *Phys. Rev. B* **81**, 245122 (2010).
29. H. Shinaoka, T. Miyake, S. Ishibashi, *Phys. Rev. Lett.* **108**, 247204 (2012).
30. Y. Yamaji, M. Imada, *Phys. Rev. X* **4**, 021035 (2014).
31. S. S. P. Parkin, M. Hayashi, L. Thomas, *Science* **320**, 190–194 (2008).

ACKNOWLEDGMENTS

We thank R. Laughlin for helpful discussions. We thank A. Bestwick, E. Fox, and D. Goldhaber-Gordon for help with the dilution refrigerator measurement. The measurement at Stanford University is supported by NSF grant DMR-1305731, the Gordon and Betty Moore Foundation through grant GBMF3133, and Emergent Phenomena in Quantum Systems (EPiQS) initiative GBMF4546. The crystal growth at University of Tokyo and RIKEN is supported by the Grant-in-Aid for Scientific Research (grant 80609488 and 24224009) from the Japan Society for the Promotion of Science and the Funding Program in World-Leading Innovative R&D on Science and Technology (FIRST Program). S.T. is partly supported by China Scholarship Council (grant 201304910185). K.C. is supported by the National Young 1000 Talents Program and the National Science Foundation of China (NSFC) under contract 51302207. The Advanced Light Source is supported by the director, Office of Science, Office of Basic Energy Sciences, Materials Sciences Division, of the U.S. Department of Energy under contract DE-AC02-05CH11231 at Lawrence Berkeley National Laboratory and University of California, Berkeley, California. All additional data are available in the supplementary materials. Z.-X.S. is a cofounder of PrimeNano Inc., which licensed the sMIM technology from Stanford for commercial instrument. This technology was modified for low-temperature measurement in this report. Stanford University and RIKEN have filed a joint provisional U.S. patent application on memory devices based on conductive magnetic domain walls.

SUPPLEMENTARY MATERIALS

www.sciencemag.org/content/350/6260/538/suppl/DC1
Materials and Methods
Figs. S1 to S8

19 June 2015; accepted 22 September 2015
10.1126/science.aac8289

Mobile metallic domain walls in an all-in-all-out magnetic insulator

Eric Yue Ma *et al.*

Science **350**, 538 (2015);
DOI: 10.1126/science.aac8289